Nonradial oscillations in classical pulsators. Prospects for seismology

Wojciech Dziembowski[1,2] **and Radosław Smolec**[1]
[1] Nicolaus Copernicus Astronomical Center, Warsaw, Poland
[2] Warsaw University Observatory, Warsaw, Poland

Data and a new interpretation

Excitation of non-radial modes in classical pulsators was predicted nearly 40 years ago (Dziembowski 1977, Osaki 1977). However, only recently, the prediction has been confirmed with the detections of a secondary periodicity at $P_x \in (0.60,\ 0.65)P_{1O}$ in a significant fraction of RRc stars and 1O Cepheids (eg. Gruberbauer et al. 2007, Soszyński et al. 2010, Netzel et al. 2015). In the Petersen diagram – **Fig. 1** – these variables form separate sequences. Interestingly, in many stars frequency peaks at $1/2\nu_x$ are also observed and were initially interpreted as sub-harmonics – manifestation of period doubling of the additional mode (Moskalik et al. 2015).

In Dziembowski (2016) we presented a new interpretation, in which the signal at $1/2\nu_x$ corresponds to p_0 modes of moderate degrees, $\ell = 7,\ 8,\ 9$, while the typically higher signal at ν_x is its harmonic. We call these objects, respectively, **1On Cepheids** and **RRcn stars**. In the latter, we do not see the $\ell = 7$ signals. Instead, we do see the $\ell = 8 + 9$ combination peaks. The secondary peaks are often broad but particularly those at $1/2\nu_x$ – see **Fig. 2**, which may be in part attributed to the excitation of p_0 modes with the same ℓ but different azimuthal degree, m. We see here the chances for measuring the mean rotation rates in stellar envelopes once suitable data are available.

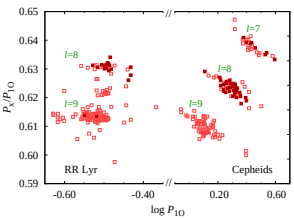

Fig. 1. Petersen diagram for RR Lyr stars and classical Cepheids. In stars marked with filled symbols, signal at $1/2\nu_x$ was detected (from Smolec & Śniegowska 2016).

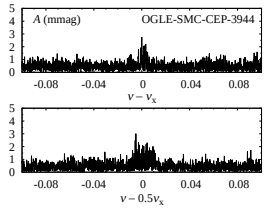

Fig. 2. Illustration of typical structure of frequency peaks detected at ν_x (top) and at $1/2\nu_x$ (bottom).

Why data on the harmonics are superior

We consider pulsation in slowly rotating spherical envelopes. Then the surface distortion caused by the excitation of the ℓ-degree multiplet is given by:

$$\frac{\delta R_\ell}{R} = P_\ell^0 \epsilon_{z,\ell}\cos(\alpha_{z,\ell} - \omega_\ell^j t) + \sum_j P_\ell^j \Big(\epsilon_{p,\ell}^j \cos\left[\alpha_{p,\ell}^j - \omega_\ell t + j(\phi - (1 - C_\ell)\Omega t)\right] + \epsilon_{r,\ell}^j \cos\left[\alpha_{r,\ell}^j - \omega_\ell t - j(\phi - (1 - C_\ell)\Omega t)\right]\Big), \quad (1)$$

where $P_\ell^{j=|m|}$ is the Legendre function, normalized in such a way that each of the ϵ-s represents contribution to the r.m.s. of the distortion. C_ℓ is the Ledoux constant and Ω is the rotation frequency. At the level of linear theory, ϵ-s and the respective phases, α-s, remain arbitrary. The associated bolometric flux variations are given by:

$$\delta F_\ell = F|f|\left(\frac{\delta R_{\ell,f}}{R}\right) \quad (2)$$

where the complex coefficient f is obtained directly from linear non-adiabatic calculations and $\delta R_{\ell,f}$ is given by the expression same as (1) but with all the phases shifted by $\arg(f)$. Given f, the variations in specified pass-band may be found from tabular data on the static plane-parallel atmosphere models. Within the **linear approximation**, calculations of stellar magnitude variations seen by the inertial observer yield

$$\mathcal{M}_{\ell,1} \approx b_{\ell,1}\Big[\left(\frac{\delta F_\ell}{F}\right) + (\ell - 2)(\ell + 1)\left(\frac{\delta R_\ell}{R}\right)\Big]. \quad (3)$$

Above, δR_ℓ and δF_ℓ should be evaluated at the observer's coordinates and $b_{\ell,1}$ is disc averaging factor weighted with limb-darkening function. Its ℓ dependence is illustrated in **Fig. 3**. It rapidly drops at low ℓ values. At higher ℓ, the decline is slower. Asymptotically $b_{\ell,1} \sim \ell^{-1/2}$ for even ℓ and $b_{\ell,1} \sim \ell^{-3/2}$ for odd ℓ.

Amplitude of the harmonics. The most obvious and likely dominant effect arises from the non-linearity of the flux-radius relation. The **quadratic effects** give rise to spherically symmetric flux variations at **the harmonic frequencies.** The resulting magnitude variations are given by:

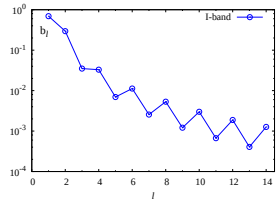

Fig.3. Disc averaging factor as a function of mode degree, ℓ.

$$\mathcal{M}_{\ell,2} = a_2\overline{\left(\frac{\delta R_\ell}{R}\right)^2}, \quad (4)$$

where the value of a_2 may be estimated from observational data and/or nonlinear models of radial pulsation. From eq. (1):

$$\overline{\left(\frac{\delta R_\ell}{R}\right)^2} = \frac{\epsilon_z^2}{2}\cos(2\alpha_z - 2\omega_\ell t) + \sum_{m=1}^{l} \epsilon_p^m \epsilon_r^m \cos(\alpha_p^m + \alpha_r^m - 2\omega_\ell t). \quad (5)$$

The most important advantages of the signal at harmonic are:

- lack of reduction of the observable amplitude caused by the averaging. In contrast, the peaks at mode frequency suffer from averaging and are detected preferentially at even ℓ (Fig.1)
- all modes, regardless of m, contribute only to $2\omega_0$, leading to narrower peaks. The mode frequency is thus more accurately determined from the harmonic.

Non-radial modes in classical Cepheids

The largest sample of 138 1On Cepheids was detected in the Small Magellanic Cloud (Soszyński et al. 2010) and we focus on their modelling. The observed period ratios are easily reproduced with metallicities covering the range contemplated for the SMC – **Fig. 4**. The models follow two extreme $M - L$ relations derived from evolutionary calculations of Georgy et al. (2013). The low M/high M models correspond to the lowest/highest mass allowed at a given luminosity in the center of the IS. The models leave no doubt regarding assignment of ℓ to the three sequences: $\ell = 7$ for the top sequence, $\ell = 8$ for the middle sequence and $\ell = 9$ for the bottom sequence. For the SMC we benefit from the precisely determined distance to the system, which allows us to compare the observed and calculated reddening free magnitude, W_I – **Fig. 5**.

Considering period ratios, Fig. 4, low-mass models clearly fit the data better; metal abundance hardly matters. The low-mass models fit also better the $P - L$ diagrams, Fig. 5. The estimated masses and luminosities increase as we move from the bottom, $\ell = 9$ sequence ($M \approx 2.4 - 2.7\,\mathrm{M}_\odot$, $\log L/\mathrm{L}_\odot \approx 2.55 - 2.7$), to the top, $\ell = 7$ sequence ($M \approx 3.3 - 4.0\,\mathrm{M}_\odot$, $\log L/\mathrm{L}_\odot \approx 3.15 - 3.3$). Such models correspond to the first crossing of the instability strip. According to current models, masses are too low for the 2-nd and 3-rd crossing to occur. We see a conflict with evolutionary models here, as incidence rate of 1On Cepheids is too high to explain all these object as 1-st crossers.

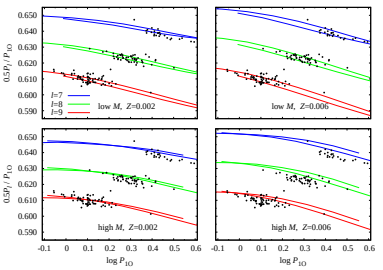

Fig. 4. Petersen diagrams for 138 1On Cepheids from the SMC confronted with model predictions for $\ell = 7$ (blue), 8 (green) and 9 (red) modes. At each degree two lines delineate the IS boundaries.

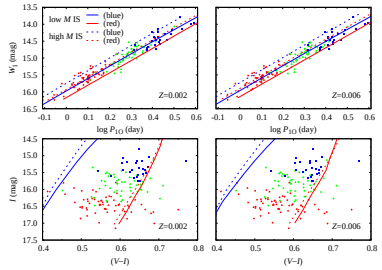

Fig. 5. Location of 138 1On Cepheids from the SMC in the period-luminosity (top) and color-magnitude (bottom) diagrams confronted with the model predictions. Stars of the top, bottom and middle sequence are plotted with blue, green and red symbols, respectively.

Non-radial modes in RR Lyrae stars

The RRcn pulsation must be common – 14 out of 15 RRc stars observed from space show this form of pulsation (eg. Moskalik et al. 2015, Molnár et al. 2015). The largest sample of RRcn stars, more than 260, was discovered in the ground-based OGLE observations of the Galactic bulge (Netzel Smolec & Moskalik 2015a,b). **Fig. 6** confronts the Petersen diagram for RRcn stars with pulsation models. The top and the bottom sequences are assigned with $\ell = 8$ and $\ell = 9$, respectively. We note that in stars of the top sequence, signal at $1/2\nu_x$ is preferentially detected (Fig. 1), in agreement with our interpretation (Fig. 3). The middle sequence – points marked with the open circles – is interpreted as due to $\nu_8 + \nu_9$ frequency combination peak (fully confirmed by the observations for stars with three frequency peaks). At $\log P_{1O}$ in the $(-0.55, -0.5)$ range, containing the majority of stars, the best fits are achieved for M close to $0.55\,\mathrm{M}_\odot$, Z close to 0.002 and $\log L/\mathrm{L}_\odot$ close to 1.5. At shorter(longer) periods models of higher(lower) Z and lower(higher) L fit better, which agrees with the well known trend of the $L(Z)$ relation.

Stars marked with crosses in Fig. 6 simultaneously pulsate in the radial fundamental mode (RRdn stars). The third pulsation mode puts additional constraint on the models and allow seismic determination of basic star's parameters. Modelling of radial modes period ratio is presented in **Fig. 7**. Analysis of Figs. 6 and 7 points that RRdn stars must be massive and metal poor.

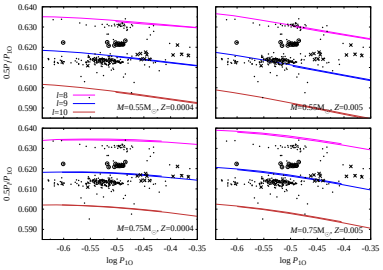

Fig. 6. Petersen diagram for RRcn stars confronted with pulsation models extending over a range of luminosities and with masses ($0.55\,\mathrm{M}_\odot$, $0.75\,\mathrm{M}_\odot$) and metallicities (0.005, 0.0004) covering the range expected for RR Lyr stars.

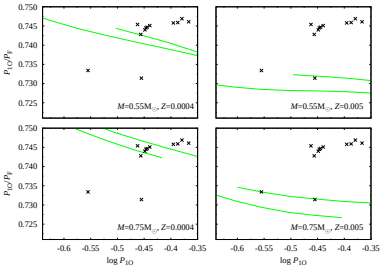

Fig. 7. Petersen diagram for two radial modes in RRdn stars. Model parameters are exactly the same as in corresponding panels of Fig. .6.

References

Dziembowski W., 1977, *Acta Astron.*, **27**, 95
Dziembowski W., 2016, *Comm. Konkoly Obs.*, **105**, 23
Georgy C., et al., 2013, *A&A*, **553**, A24
Gruberbauer M., et al., 2007, *MNRAS*, **379**, 1498
Molnár L., et al., 2015, *MNRAS*, **452**, 4283
Moskalik P., Smolec R., Kolenberg K. et al., 2015, *MNRAS*, **447**, 2348
Netzel H., Smolec R., Moskalik P., 2015a, *MNRAS*, **447**, 1173
Netzel H., Smolec R., Moskalik P., 2015b, *MNRAS*, **453**, 2022
Osaki Y., 1977, *PASJ*, **29**, 235
Smolec R., Śniegowska M., 2016, *MNRAS*, **458**, 3561
Soszyński I., et al., 2010, *Acta Astron.*, **60**, 17

NATIONAL SCIENCE CENTRE POLAND

This research is supported by the Polish National Science Center, **grant DEC-2012/05/B/ST9/03932**.